

Microtubule Binding and Trapping at the Tip of Neurites Regulate Tau Motion in Living Neurons

Carina Weissmann¹, Hans-Jürgen Reyher²,
Anne Gauthier¹, Heinz-Jürgen Steinhoff²,
Wolfgang Junge³ and Roland Brandt^{1,*}

¹Department of Neurobiology, University of Osnabrück, Barbarastraße 11, D-49076 Osnabrück, Germany

²Department of Experimental Physics, University of Osnabrück, Barbarastraße 11, D-49076 Osnabrück, Germany

³Department of Biophysics, University of Osnabrück, Barbarastraße 11, D-49076 Osnabrück, Germany

*Corresponding author: Roland Brandt, brandt@biologie.uni-osnabrueck.de

During the development of neurons, the microtubule-associated tau proteins show a graded proximo-distal distribution in axons. In tauopathies such as Alzheimer's disease, tau accumulates in the somatodendritic compartment. To scrutinize the determinants of tau's distribution and motion, we constructed photoactivatable green fluorescent protein (GFP)-tagged tau fusion proteins and recorded their distribution after focal activation in living cells. Simulation showed that the motion of tau was compatible with diffusion/reaction as opposed to active transport/reaction. Effective diffusion constants of 0.7–0.8 $\mu\text{m}^2/\text{second}$ were calculated in neurites of PC12 cells and primary cortical neurons. Furthermore, tau's amino terminal projection domain mediated binding and enrichment of tau at distal neurites indicating that the tip of a neurite acts as an adsorber trapping tau protein. Treatment with taxol, incorporation of disease-related tau modifications, experimentally induced hyperphosphorylation and addition of preaggregated amyloid β peptides ($A\beta$) increased the effective diffusion constant compatible with a decreased binding to microtubules. Distal enrichment was present after taxol treatment but was suppressed at disease-relevant conditions. The data suggest that (i) dynamic binding of tau to microtubules and diffusion along microtubules and (ii) trapping at the tip of a neurite both contribute to its distribution during development and disease.

Key words: axon, microtubule-associated protein, photoactivation, tau, tauopathy

Received 30 January 2009, revised and accepted for publication 10 August 2009, uncorrected manuscript published online 13 August 2009

The tau proteins belong to the family of microtubule-associated proteins (MAPs). They are mainly expressed in neurons where they are enriched in the axon and play major regulatory roles in the organization and integrity of the cytoskeletal network (1). The repeat region of tau in the

carboxyterminal half is the basic microtubule-interacting unit. Tau has also been shown to interact with components of the neural plasma membrane cortex through its amino terminal non-microtubule-binding domain, which protrudes from the microtubule surface when tau interacts with microtubules (2). Phosphorylation of tau affects its interaction both with microtubules and with the membrane cortex (3). The functional role of these interactions remains to be elucidated.

Alzheimer's disease (AD) is characterized by a progressive loss of neurons in certain brain regions, the accumulation of extracellular amyloid plaques formed from amyloid β ($A\beta$) peptides, and the aggregation of tau into neurofibrillary tangles (NFTs) (4). Tau mutations in familial tauopathies such as frontotemporal dementia and parkinsonism linked to chromosome 17 (FTDP-17) confirmed a central role of tau pathology in disease progression.

A key morphological feature during the development of AD and other tauopathies is the redistribution of tau from the axon into the somatodendritic compartment. Tau's redistribution is concomitant with an increased phosphorylation (hyperphosphorylation) at selected sites (5). The determinants of tau's axonal distribution and the mechanisms of its mislocation during disease are unclear. They may involve axonal transport (6,7), locally regulated binding to microtubules (8), selective stabilization in the axonal compartment (9), localization of tau mRNA to the proximal axon (10) and binding of tau to neural plasma membrane components (2).

As a microtubule-associated protein, tau may regulate microtubule-dependent mechanisms in neurons. It has been shown that overexpression of tau inhibits anterograde organelle and vesicular transport in axons (11) and that tau modulates dynein and kinesin motility (12). Tau interacts in a phosphorylation-dependent manner with the light chain of kinesin-1 and tau phosphorylation may modulate its own axonal transport (13). In turn, recent data have provided evidence that impairments in axonal transport can lead to pathological changes of tau protein (14) underlining that the analysis of tau motion in cells could contribute to a better understanding of the mechanisms of neurodegeneration.

Several techniques have been developed to study protein motion in living cells. These include fluorescence protein tracking using green fluorescent protein (GFP) variants and photobleaching to study molecular dynamics (15,16). With these methods, it became possible to determine transport rates and apparent diffusion constants of cytoskeletal proteins in living neurons (17). However, these techniques are

not sensitive enough to determine the motion of a defined subpopulation of molecules in a spatio-temporal manner. The development of photoactivatable fluorescence molecules such as photoactivatable green fluorescent protein (PAGFP) allows to focally activate a subpopulation of fluorescence-tagged molecules and to follow their distribution in unprecedented sensitivity and over longer times. This technique has, for example, been used to demonstrate interlysosomal membrane exchange (18) and to analyze flux of microtubule subpopulations (19).

To analyze tau's motion and factors that influence tau's distribution in living neural cells, we used photoactivatable GFP-tagged tau constructs and performed computer-assisted image analysis of time-lapse recordings after focal activation in neurites. We show that photoactivatable tau fusion constructs provide a useful tool to analyze the molecular dynamics of tau's interaction in neuronal compartments. We demonstrate that tau's distribution in neurites is governed by diffusion/reaction as opposed to active transport/reaction. The effective diffusion constant equals its true diffusion constant times the fraction of free tau over total tau. Furthermore, we show that tau's amino terminal projection domain mediates binding and enrichment of tau at distal neurites thereby trapping tau at the tip of a neurite. Disease-relevant conditions such as experimentally induced hyperphosphorylation or treatment with A β reduce microtubule binding and abolish the distal enrichment.

Results

Fluorescence photoactivation reveals fast distribution of tau on cellular microtubules

We examined the dynamics of tau's subcellular distribution using a fluorescence photoactivation approach in rat neural pheochromocytoma cell lines (PC12) and primary mouse cortical neurons. Cells were transfected with fusion constructs of the photoactivatable green fluorophore PAGFP (18) and human tau (PAGFP-wt tau) (Figure 1A, left). In addition, a pseudohyperphosphorylated (PHP) tau variant, which mimics AD-like hyperphosphorylation (20), and a tau deletion construct (tau Δ) lacking the microtubule binding region (MBR) were used. 3XPAGFP was prepared as a cytosolic, non-tau-related control because it separated at the same apparent molecular weight as PAGFP-wt tau (Figure 1A, middle). In contrast to shorter PAGFP constructs, 3XPAGFP was completely cytosolic. Wt tau but not tau Δ were immunoreactive against the Tau5 antibody, which recognizes an epitope that is only partially included in tau Δ (21) (Figure 1A, right).

The green fluorescence of PAGFP was monitored in a confocal laser scanning microscope (cLSM) using an excitation wavelength of 488 nm (Figure 1B). PAGFP was activated in a focal spot of the cell by a laser flash at 405 nm wavelength. Time-lapse imaging after activation of a spot in the cell body of living PC12 cells

expressing 3XPAGFP or PAGFP-wt tau revealed that the fluorescence quickly decreased at the site of photoactivation (Figure 1C,D). The total fluorescence of the cell did not decrease within the time of analysis (112 seconds) indicating high photostability and only low reversal of photoactivation (Figure 1C). In neuronally differentiated PC12 cells, PAGFP-wt tau appeared locally bound shortly after photoactivation (3 seconds) and thereafter distributed on filamentous structures (7 and 112 seconds) throughout the cell, whereas tau Δ distributed homogeneously in the cytoplasm (Figure 1D), similarly to 3XPAGFP. Double immunofluorescence microscopy of a fixed and focally activated PAGFP-wt tau expressing cell revealed partial co-localization of photoactivated tau with microtubules (Figure 1E). This indicates that the PAGFP fusion does not interfere with the ability of tau to bind to the microtubule array in the cell. The data indicate that photoactivatable tau fusion constructs provide a useful tool to analyze the molecular dynamics of tau's cellular interactions.

Tau's dissipation fits a diffusion model and an amino terminal tau fragment exhibits a transient enrichment in the tip of neurites

We next investigated protein distribution in neurites of transfected and differentiated PC12 cells. For these experiments, PC12 cell lines were produced that stably expressed the different PAGFP fusion constructs (see Figure 1A). Cell lines with similar expression levels ($\sim 1-2 \times 10^7$ molecules/cell, corresponding to about 20–40 pmol/ 10^6 cells) were selected. Such an expression level is in the range of endogenous tau expression in neurons (22). The cells were differentiated with nerve growth factor (NGF) and photoactivated in the middle of the neurite (Figure 2A). To visualize and evaluate the protein distribution in a spatio-temporal manner, low-resolution imaging followed by computer-assisted image analysis of the time-lapse recordings was performed. The contour of the cell was recognized, a region of interest (ROI), which included the neurite under investigation, was selected and main axes were calculated as described in *Materials and Methods*. To visualize the distribution over time, the two-dimensional (2D) intensity function $I(x, t)$ with projection coordinate x and time t was plotted as a color-coded filled contour plot. It should be noted that $I(x)$ represents the intensity density (per pixel) projected to the neurite's axis, thereby correcting the fluorescence intensity for local changes in the thickness of the neurite. In addition, the decay of fluorescence intensity in the activated segment was simulated by a diffusion model assuming an infinite tube with one closed end (see *Materials and Methods*).

Photoactivation of PAGFP-wt tau expressing PC12 cells in the middle of a neurite triggered an increase in fluorescence (PAGFP*-wt tau) that symmetrically dissipated in both directions (Figure 2B, top left). In the majority of the cells (86%, $n = 30$), the position of the maximum of the activated segment remained at the same position (43% of the cells) or moved slightly toward the cell

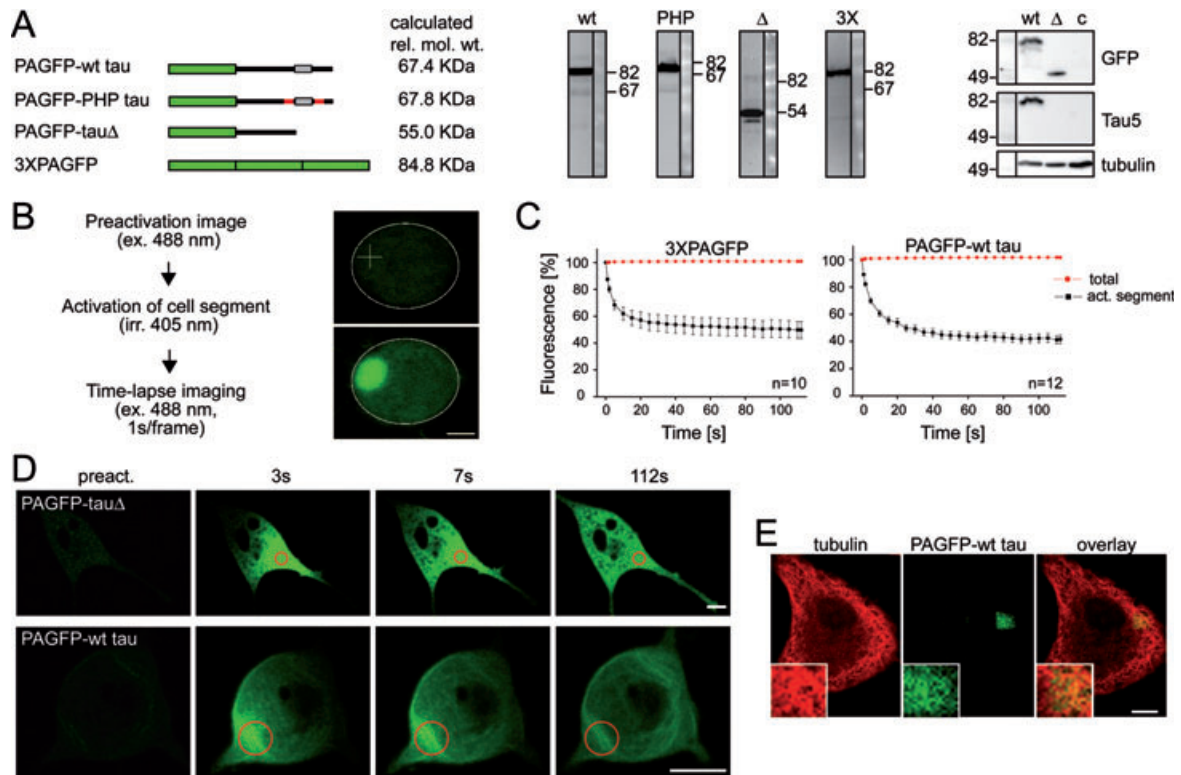


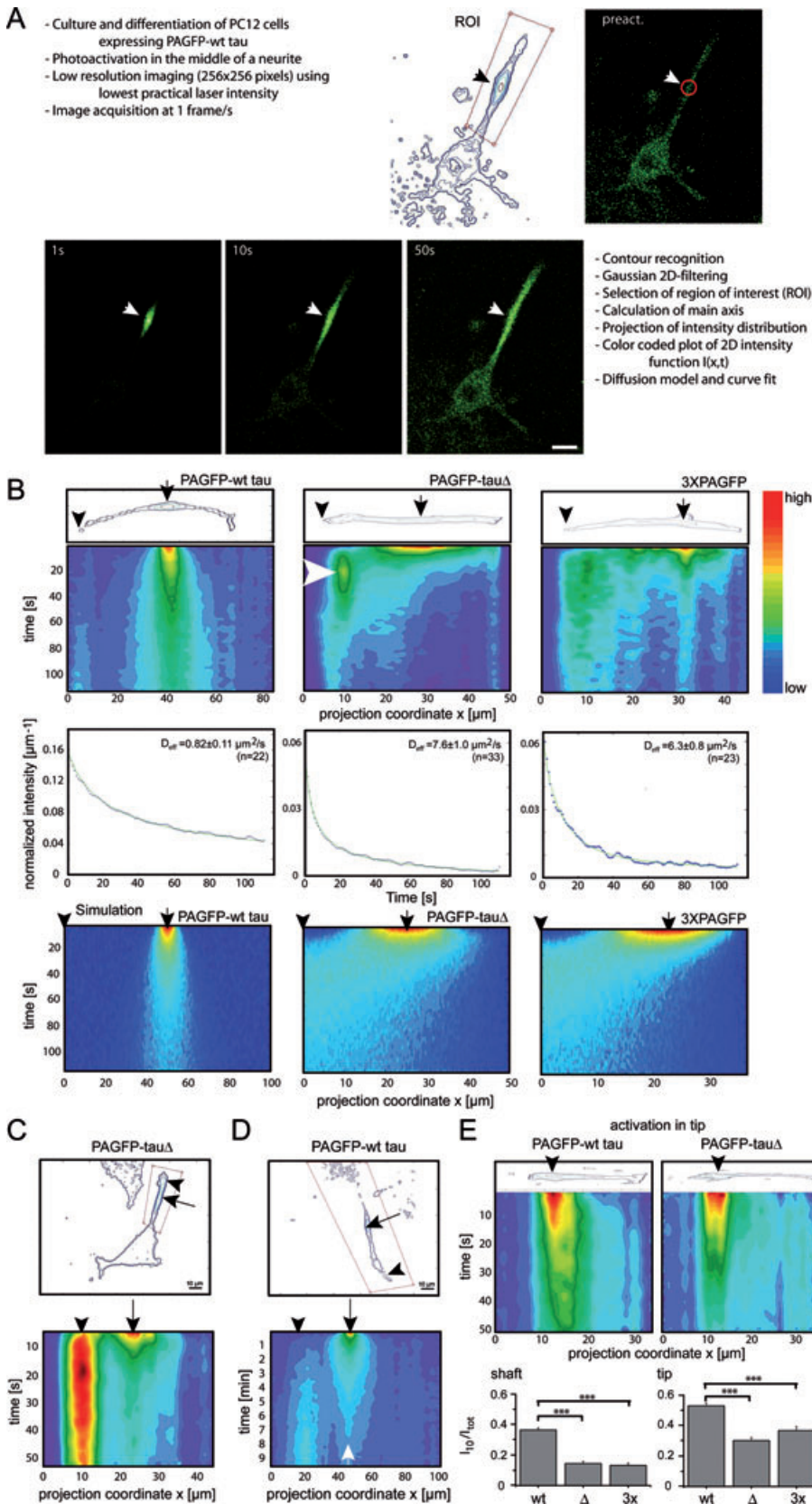
Figure 1: Fluorescence photoactivation reveals fast distribution of tau on cellular microtubules. A) Schematic representation of PAGFP tau fusion constructs and 3XPAGFP as a cytosolic control. The MBR is indicated as gray box. Regions that are mutated in PHP tau according to (20) are indicated in red. Immunoblots of lysates of PC12 cells stably expressing the different constructs are shown. Constructs were detected using polyclonal anti-GFP antibody (middle) or antibodies as indicated (right). Note that PAGFP-tau Δ does not react with the Tau5 antibody. B) Experimental set-up and photoactivation of a segment in the cell body of a fixed, undifferentiated PC12 cell expressing 3XPAGFP. The outline of the cell and the position of activation are indicated. Scale bar, 5 μ m. C) Fraction of fluorescence measured in the activated segment and total fluorescence of living PC12 cells expressing 3XPAGFP or PAGFP-wt tau. Mean \pm SEM are shown. D) Images of differentiated PC12 cells expressing PAGFP*-tau Δ and PAGFP*-wt tau demonstrating fast distribution of full-length tau on the microtubule array due to the presence of the MBR. The position of activation is indicated by a red circle. Scale bars, 10 μ m. E) Double fluorescence micrograph of a detergent-extracted and fixed PC12 cell demonstrating partial colocalization of PAGFP*-wt tau with microtubules (yellow color in overlay). The activated region is shown at higher magnification in the inserts. PAGFP-tau Δ and 3XPAGFP did not colocalize with microtubules in similar experiments. Scale bar, 10 μ m.

body (43% of the cells) during the observation period. In the remaining 14% of the cells, a slight movement toward the tip of the process was observed (Figure S1). Thus, the data indicate the absence of active directed transport (fast axonal transport) involving motor proteins. The decay of the fluorescence intensity in the activated segment could be well simulated by a diffusion model with an effective diffusion coefficient (D_{eff}) of $0.82 \pm 0.11 \mu\text{m}^2/\text{second}$ ($n = 22$) (Figure 2B, middle left). Simulation with a closed tube model fitted well the dissipation of tau justifying the assumption that tau binding and release rates are much faster than diffusion, which reduces the reaction-diffusion equations to a simple diffusion equation with an effective diffusion constant (23) (Figure 2B, bottom left).

PAGFP*-tau Δ dissipated much faster than full-length tau (Figure 2B, middle) with an almost 10-fold higher D_{eff} indicating that binding via the MBR mediates reduced diffusion of full-length tau. In agreement, 3XPAGFP*

distributed with a D_{eff} similar to tau Δ (Figure 2B, right). We did not observe a significant change of process lengths during the measurements indicating that the calculated effective diffusion coefficients are not altered by process growth or retraction. The diffusion of 3XPAGFP or tau Δ in neurites was lower than the diffusion of GFP in different cell models where values between 15 and 87 $\mu\text{m}^2/\text{second}$ had been calculated based on fluorescence recovery after photobleaching (FRAP) experiments (17,24,25). However, measurements of diffusion constants in the nucleus have revealed that triple (EGFP) has a less than half as high effective diffusion coefficient compared with the EGFP monomer (26). From this, it can be concluded that 3XPAGFP diffusion in the process is equal or only slightly lower than in other compartments of the cell.

Surprisingly, we also observed in many neurites of PAGFP-tau Δ -expressing cells a transient enrichment of PAGFP*-tau Δ close to the tip of the neurite shortly after



photoactivation in the middle of the process (Figure 2B, middle, white arrow; Figure S2). Transient enrichment was evident by the presence of a local minimum between enrichment and activation zone and occurred in the majority (57%; $n = 23$) of neurites with photoactivated PAGFP-tau Δ . No transient enrichment was present in similar experiments with the cytosolic control protein 3XPAGFP* (Figure 2B, right; Figure S3). It should be noted that the presence of a closed end results in a transient increase of the concentration of 3XPAGFP* in the distal neurite which could also be simulated with a closed tube model matching the experimental time range (20–60 seconds) and geometry (Figure 2B, bottom). However, the difference between enrichment and increased concentration at the tip consists in the important fact that an intensity distribution simulated by isotropic diffusion alone never can show a local minimum between activation zone and any second region. Thus, the presence of a local minimum implies an intensity gradient directed from the tip indicating that the tip acts as an adsorber trapping tau's amino terminal projection domain or that tau Δ is carried by active anterograde transport. The extent of distal enrichment varied between cells and was strongest in neurites with growth cones that covered larger areas (Figures 2C and S2), indicating that trapping of tau is more efficient in large growth cones. It should be noted that the shape of the tube cap, that is, the form of the neurite tip, will alter the temporal behavior of the transient enrichment, because the boundary condition is then modified. However, a cone or any more complicated taper can never lead to a local minimum between tip and activation area, because this is physically contradictory to an isotropic diffusion process.

Movement of tau is compatible with diffusion/reaction as opposed to active transport/reaction

Distal enrichment of PAGFP-tau Δ as observed in our experiments could be caused by active anterograde transport or by diffusion in combination with the presence of an adsorber at the tip. To distinguish between these possibilities, we determined the average velocity, v_e , with which PAGFP*-tau Δ , which had been activated in the middle of the process, reached the tip of the neurite. v_e was calculated as $\Delta x/\Delta t$, where Δx is the distance between enrichment and activation zone and Δt is the time when the enrichment maximum is observed. We found $v_e = 0.94 \pm 0.22 \mu\text{m}/\text{second}$ for short processes (tip at a mean distance of $14.0 \pm 2.1 \mu\text{m}$) and $v_e = 1.33 \pm 0.16 \mu\text{m}/\text{second}$ for longer processes (tip at a mean distance of $39.0 \pm 3.1 \mu\text{m}$). For active transport, the same velocities would be expected independent of the distance. More importantly, the velocity is much lower than expected for fast axonal anterograde transport (2–5 $\mu\text{m}/\text{second}$) (27). Furthermore, treatment of cells with iodoacetate, which inhibits the glycolytic enzyme glyceraldehyde-3-phosphate dehydrogenase (28) and reduces cytosolic ATP, did not affect the distribution of PAGFP*-tau Δ . Thus, the data indicate that distal

enrichment is independent of motor protein activity and is due to the presence of an adsorber at the tip.

Previously it has been shown that tau is a component of slow axonal transport and transport rates between 0.2 and 3 mm per day have been reported (29–33). To determine a potential slow transport of tau in neurites of PC12 cells, we performed additional photoactivation experiments in which we increased the observation time from 112 seconds to 10 min. We did not observe a net movement of the peak of PAGFP*-wt tau toward the tip of the neurite (Figure 2D). Instead, we observed a mean displacement of $0.65 \pm 4.94 \mu\text{m}$ toward the cell body ($n = 11$). Assuming a slow axonal transport rate of 1 mm/day as it has been previously reported for rat cortical cultures (31), about 7 μm of displacement during the observation period would be expected. Thus, we did not obtain evidence for movement of tau by slow axonal transport in our system.

To determine whether tau is specifically retained in distal neurites, we performed additional experiments where we monitored fluorescence distribution after photoactivation in the tip region. Dissipation after activation in the tip was lower for wt tau as well as for tau Δ compared with dissipation from the middle of the process as evidenced by a slower decay of the fluorescence in the activated region (Figure 2E, top). To quantitate the decay of fluorescence, an immobile fraction, I_{10}/I_{tot} , was determined by calculating the fluorescence intensity in the activated segment at 10 seconds post-activation (I_{10}) relative to total fluorescence that was initially activated (I_{tot}). I_{10}/I_{tot} was higher for all constructs in the tip compared with the shaft (Figure 2E, bottom) indicating reduced mobility in the tip region. Moreover at the tip, wt tau was significantly less mobile than tau Δ or 3XPAGFP suggesting that microtubule anchorage is the major mechanism that restricts tau's mobility at the tip. It should be noted that we did not observe a significant difference between the mobility of tau Δ and 3XPAGFP in the tip indicating that trapping of tau Δ by binding to an adsorber is weak compared with the effect of the physical restriction caused by the nearby end of the neurite. Thus, the results suggest that trapping of tau by binding to an adsorber will, only in combination with microtubule binding, lead to a more permanent enrichment of proteins at the distal neurite.

To determine whether binding of tau Δ to the tip interferes with endogenous tau distribution, cells were transfected with PAGFP-tau Δ , fixed and stained for endogenous tau and PAGFP-tau Δ . In transfected cells, tau Δ was clearly present at the distal tips of neurites consistent with its trapping in growth cones (Figure 3, top row, middle). While endogenous tau was present in the processes of cells that did not express tau Δ (Figure 3, bottom row), tau appeared to be less prominent in neurites in tau Δ -expressing cells suggesting that tau Δ and endogenous tau compete for the same binding site.

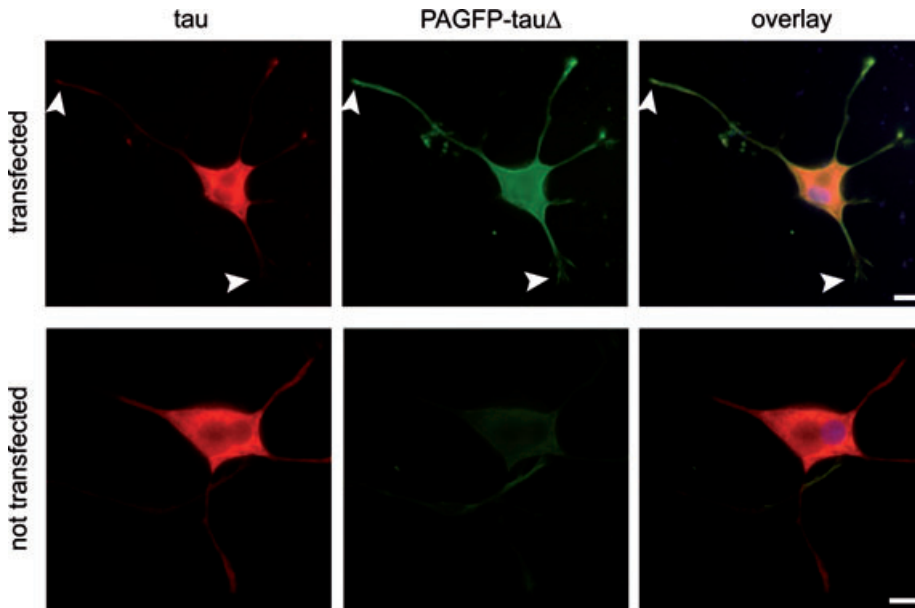


Figure 3: Distribution of endogenous tau and an amino terminal tau fragment in differentiated PC12 cells. Fluorescence micrographs of differentiated PC12 cells that have been transfected (top) or not transfected (bottom) with PAGFP-tau Δ . Cells were fixed and stained for endogenous tau with Tau5 antibody, which does not react with tau Δ (see Figure 1A). Transfected cells were identified with an antibody against GFP. Arrowheads indicate neurites that stain for tau Δ but only weakly for endogenous tau (top) compared to not transfected cells. Scale bars, 10 μ m.

Tau diffuses and shows transient enrichment at the distal tip in axons of primary cortical neurons

PC12 cells extend neurites and resemble neurons in many aspects but do not develop axonal-somatodendritic polarity. To determine whether tau diffusion and distal enrichment occur similarly in axons of primary neurons, cortical mouse cultures were prepared, transfected with PAGFP-wt tau or -tau Δ , and analyzed following photoactivation. In order to identify neurons and their axons, MAP2 stainings of control cortical cultures were performed and individual cells were imaged at high resolution (34). The morphological criteria were used to identify axons in the live imaging experiments. In agreement with our results using PC12 cells, dissipation of the tau constructs could be well fitted by a diffusion model (Figure 4A,B). Moreover in primary neurons, the D_{eff} of PAGFP-wt tau was much lower than the D_{eff} of PAGFP-tau Δ . More importantly, a transient enrichment of PAGFP*-tau Δ at the distal axon with a clear local minimum between activation and enrichment zone was also evident in the majority of transfected neurons (67%, $n=6$) (Figure 4B, white arrow), whereas it was not observed in neurons expressing 3XPAGFP. The data indicate that tau's amino terminal projection domain mediates binding of tau at the tip of an axon in a similar fashion as it was observed in transfected and neuronally differentiated PC12 cells.

Interaction with microtubules and disease-relevant conditions affect tau's diffusion and suppress enrichment of tau at the distal neurite

To determine the factors that affect tau distribution in neurites, we tested first whether microtubule interaction accounts for the reduced mobility of wt tau. Dissipation of tau from the activated segment was measured in cells that had been treated with the microtubule-disrupting

drug colchicine or with taxol, a drug that suppresses microtubule (MT) dynamics and induces detachment of tau from microtubules (35). Colchicine treatment led to a breakdown of the microtubule array and increased mobility of wt tau but not of tau Δ or 3XPAGFP indicating that intact microtubules and interaction with tau's MBR are required to restrict the diffusion of tau in neurites (Figure 5A, left). Treatment with taxol suppressed microtubule dynamics as evidenced by an increase in the fraction of acetylated tubulin as a marker for stable microtubule subpopulations (Figure 5A, right, insert). Treatment with taxol also led to an increased mobility of wt tau without affecting the mobility of tau Δ or 3XPAGFP (Figure 5A, right) confirming that tau-microtubule interaction is the major mechanism that restricts tau's mobility in neurites.

It is known that phosphorylation affects the interaction of tau with microtubules and local changes in the extent of phosphorylation may regulate tau's mobility in neurites. To measure the mobility of tau species with increased phosphorylation, PAGFP-wt-tau-expressing cells were treated with the phosphatase inhibitor okadaic acid (OA) and compared with cells that stably express pseudohyperphosphorylated (PHP) tau, which mimics AD-like hyperphosphorylation (20). PHP tau was more mobile in neurites than wt tau, and OA increased the mobility of wt tau but not of PHP tau or tau Δ (Figure 5B), indicating that tau's phosphorylation state affects its mobility by regulating tau's binding to microtubules. Furthermore, treatment with preaggregated A β 42 increased the mobility of full-length tau but not of tau Δ (Figure 5C) consistent with previous data showing that A β mediates neurotoxicity by increased phosphorylation of tau which reduces the interaction of tau with microtubules (34). The decay of the fluorescence intensity in the activated segment after treatment with A β or OA could again be well fitted by a diffusion model (Figure 5D) indicating that tau's

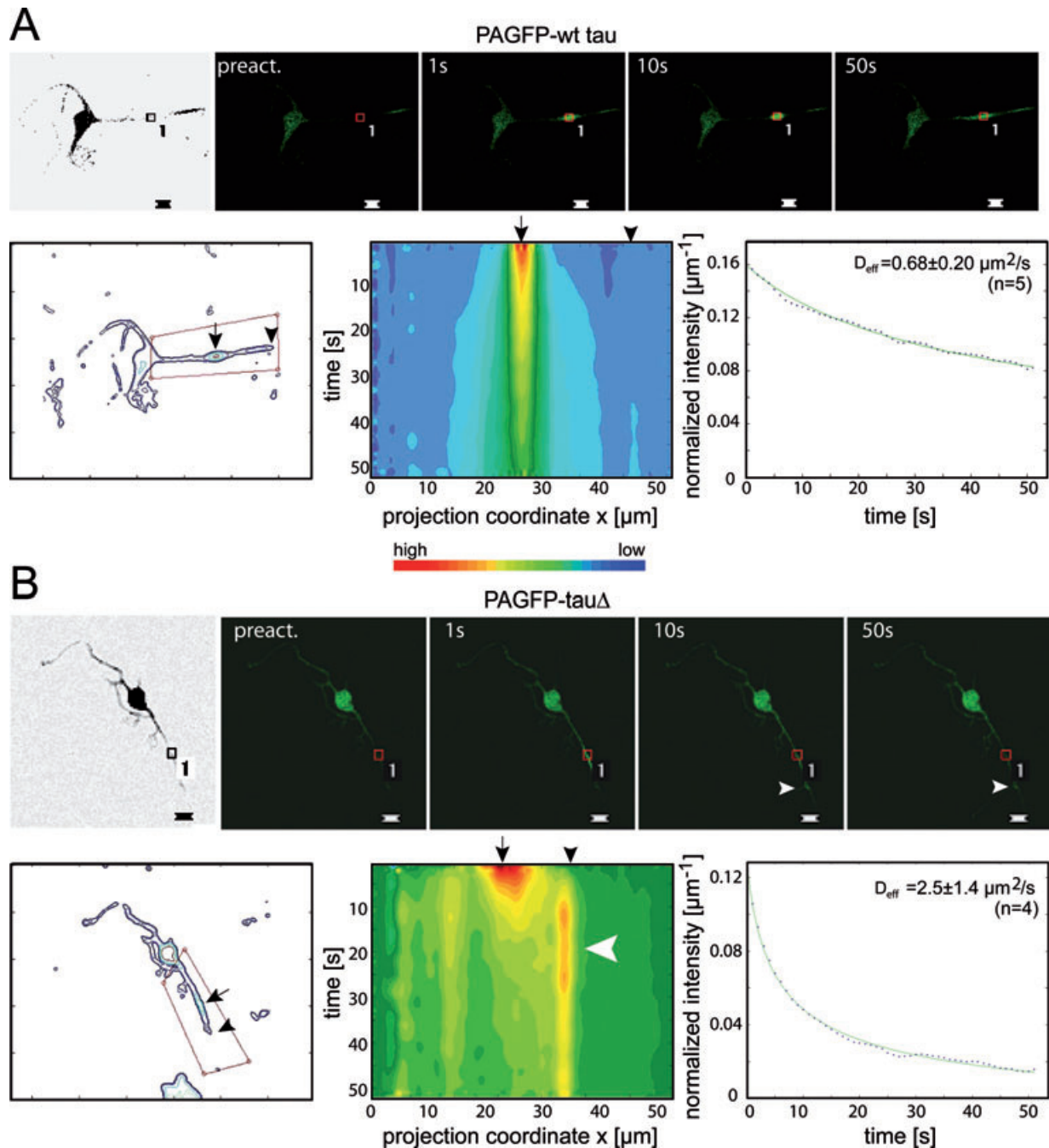


Figure 4: Tau diffuses and shows transient enrichment at the distal tip also in the axons of primary cortical neurons. A, B) Inverted image to reveal cell morphology, fluorescence micrographs of time-lapse recordings, contour and color coded plots of 2D intensity function, and fits of representative decay plots to model diffusion are shown for PAGFP*-wt tau (A) and PAGFP*-tau Δ (B). Mean effective diffusion coefficients from fits of n processes are given. Position of activation (arrow) and tip of processes (arrowhead) is indicated. Scale bar, 10 μm . Transient enrichment of amino terminal tau sequence at the tip of axons from primary neurons is indicated by a white arrowhead.

diffusivity in neurites is directly regulated by its interaction with microtubules and is increased with disease-relevant modifications and at conditions that induce tau hyperphosphorylation. Furthermore, the fit indicates that also at disease-relevant conditions microtubule binding

and release is much faster than diffusion. Using the diffusion coefficient of 3XPAGFP as a non-binding control (D_t) and the D_{eff} values for the different scenarios, the percentage of MT-bound tau can be calculated from $D_t/D_{\text{eff}} = 1 + K^*$ with K^* as the ratio of bound to free

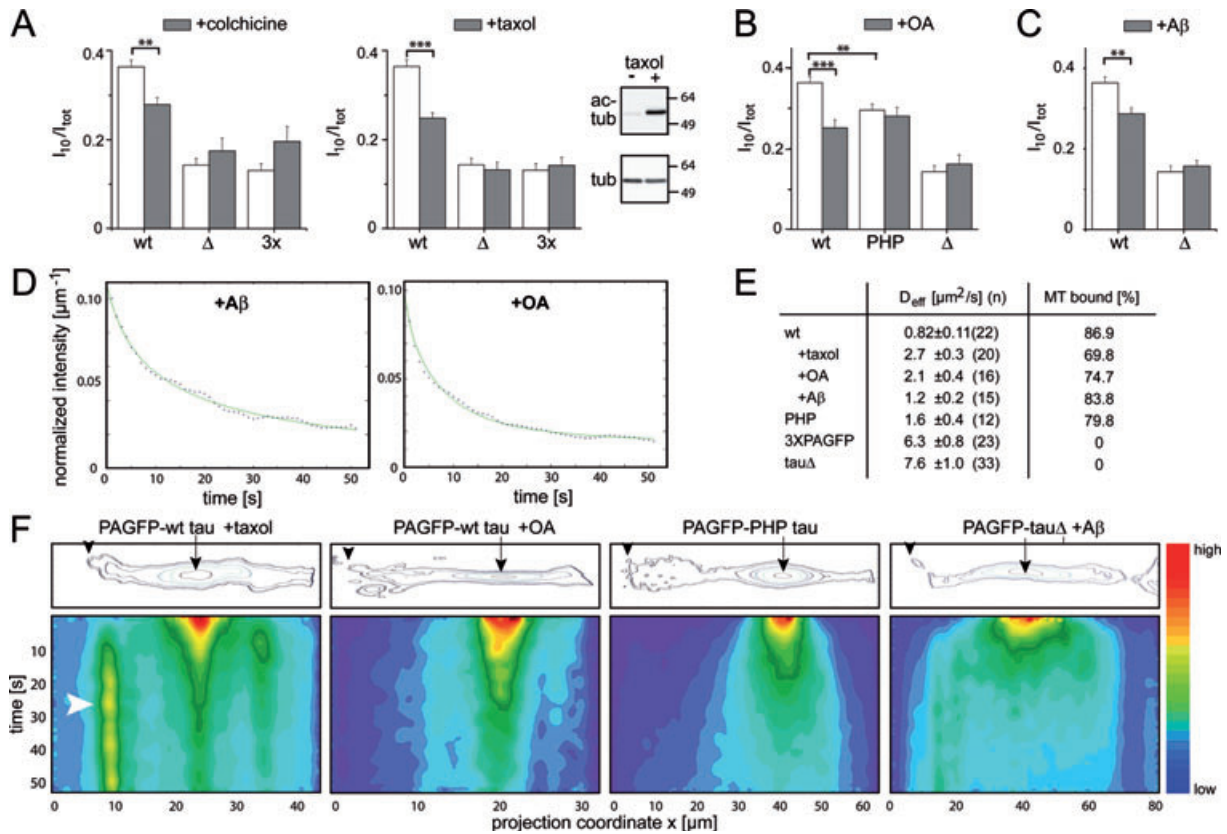


Figure 5: Interaction with microtubules and disease-relevant conditions affect tau's diffusion and suppress enrichment of tau at the distal neurite of differentiated PC12 cells. A) Effect of colchicine and taxol on immobile fractions (I_{10}/I_{tot}) demonstrating that microtubule interaction restricts the diffusion of PAGFP*-wt tau but not of PAGFP*-tau Δ or 3XPAGFP* in neurites. Mean \pm SEM, $n = 7$ –29. Immunoblots of lysates detected with antibodies against total tubulin (tub) and acetylated tubulin subpopulation (ac-tub) indicating increased microtubule stabilization in the presence of taxol are shown at the right. B) Immobile fractions of PAGFP*-wt tau, PAGFP*-PHP tau and PAGFP*-tau Δ and effect of OA. OA increases the mobility of PAGFP*-wt tau but not of the more mobile PAGFP*-PHP tau or PAGFP*-tau Δ . Mean \pm SEM, $n = 13$ –29. C) Effect of preaggregated A β on immobile fractions of PAGFP*-wt tau and PAGFP*-tau Δ demonstrating the induction of increased tau mobility of PAGFP*-wt tau at AD-relevant conditions. Mean \pm SEM, $n = 10$ –33. D) Fits of representative decay plots to model diffusion in the presence of A β or OA are shown. E) Calculation of mean effective diffusion coefficients from fits of n processes and fraction of MT-bound tau at different conditions. F) Contour and color coded plots of 2D intensity function demonstrating transient enrichment of PAGFP*-wt tau after taxol treatment at the tip of a process (white arrowhead). No transient enrichment was observed after treatment of PAGFP*-wt tau expressing cells with OA, with PAGFP*-PHP tau expression, or after treatment of PAGFP*-tau Δ expressing cells with A β . Position of activation (arrow) and tip of process (arrowhead) is indicated.

molecules (25). The calculations indicate that the majority of tau (87%) is bound to microtubules at control conditions, whereas taxol, OA or A β increase the amount of unbound tau by 3–17% (Figure 5E).

The presence of a distal enrichment with tau Δ but its absence with 3XPAGFP suggests that tau's aminoterminal specifically mediates transient binding in distal neurites. However, full-length tau did not show such a clear transient enrichment in similar experiments (Figure 2B, left, Figures 4A and S1) although some enrichment could be observed after longer observation times (see Figure 2D). Therefore, we hypothesized that this deficit was due to tau's low mobility caused by microtubule anchorage which prevents, in the analyzed time frame,

the diffusion that is required to reach the distal neurite. Consistent with our hypothesis, treatment of the cells with taxol to increase tau's mobility by reducing its binding to microtubules resulted in a transient enrichment of PAGFP*-tau in distal neurites in the majority of neurons (56%, $n = 18$) (Figure 5F, left; Figure S4).

To test whether distal enrichment is sensitive to disease-relevant conditions, we determined the effect of OA on the distribution of PAGFP*-wt tau. In contrast to the treatment with taxol, we did not observe distal enrichment of tau in OA-treated cells despite the fact that both treatments reduced tau's microtubule anchorage to a similar extent (Figure 5F, middle left). Furthermore, OA treatment also reduced the fraction of cells with distal enrichment

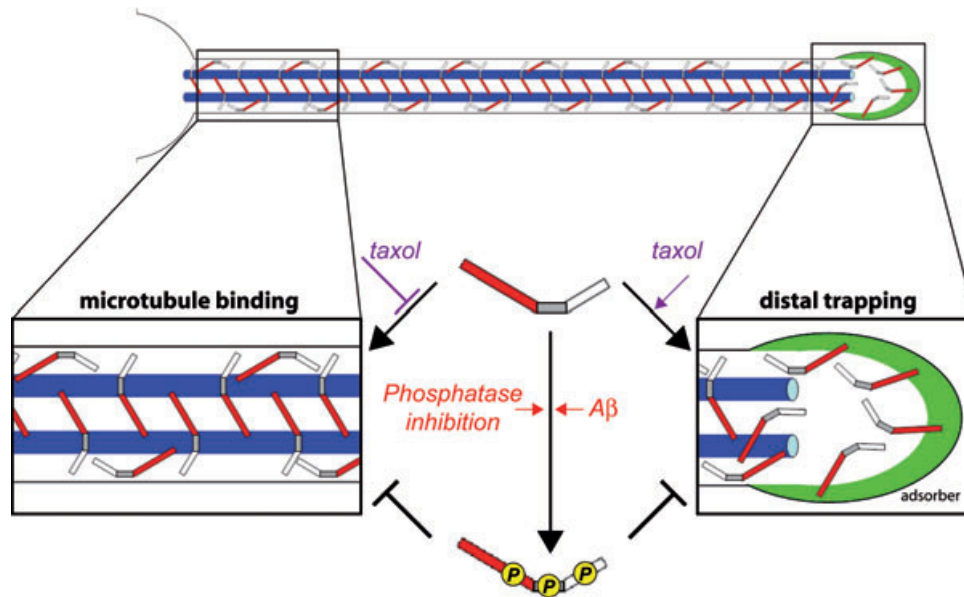


Figure 6: Model showing the mechanism of tau distribution in axons as revealed by our fluorescence photoactivation approach. Tau dynamically binds to microtubules (blue) via its MBR (gray). In the growth cone, tau's amino terminal projection domain (red) binds to an adsorber at the tip (green) causing, together with microtubule anchorage, trapping at the distal neurite. Disease-related structural changes of tau, experimentally induced hyperphosphorylation or taxol reduce tau's microtubule binding in the neuritic shaft. While taxol increases distal trapping, disease-related drugs abolish it thus causing mislocalization of tau to the somatodendritic compartment.

of PAGFP*-tau Δ (7% compared with 57% at control conditions; $n = 14$ and 23, respectively, Figure S5), indicating that experimentally induced hyperphosphorylation suppresses trapping of tau at the tip of a neurite. Distal enrichment was also absent in cells expressing PAGFP-PHP tau (Figure 5F, middle right), suggesting that conformational changes that are induced by phosphorylation of tau reduce binding to the adsorber. Treatment with preaggregated A β reduced the fraction of cells with distal enrichment of PAGFP-tau Δ to 37% ($n = 27$) (Figures 5F and S6).

It cannot be excluded that the changes in the distribution of tau are caused by indirect effects, for example, an increased degradation of the constructs in the presence of OA or after treatment with A β . To test this hypothesis, focal activation of PAGFP-tau constructs was performed and the total fluorescence of the entire cell was determined for 2 h. Fluorescence of the full-length tau construct decreased by $6.5 \pm 2.4\%$ ($n = 5$) indicating high proteolytic stability. Treatment with taxol or OA did not affect the decrease in fluorescence (decrease of $5.9 \pm 2.5\%$ and $7.2 \pm 1.9\%$, respectively) suggesting that tau's turnover is not sensitive to such a treatment. However, treatment with A β resulted in a decrease of fluorescence by $13.9 \pm 1.4\%$ ($n = 5$) indicating increased degradation of the PAGFP-wt tau fusion protein. A β -induced degradation of tau is in agreement with previous data (36) and suggests that a photoactivation approach could also be useful to analyze tau turnover in cells.

Taken together, our data indicate that the transient enrichment of tau at distal neurites is critically affected by AD-relevant conditions and is abolished after experimentally induced tau hyperphosphorylation.

Discussion

We have shown that tau's distribution in neurites fits a diffusion/reaction model, such that its effective diffusion constant is modulated by its dynamic interaction with microtubules. The effective diffusion constant equals its true diffusion constant times the fraction of free tau out of total tau (free and bound tau). From the diffusion constants, it could be calculated that the majority (87%) of tau is bound to microtubules in the cells. This observation is in agreement with estimations from biochemical fractionation experiments of endogenous and transfected tau in PC12 cells where the majority (>80%) of tau has been found to be associated with microtubules (37).

From calculations of FRAP experiments, a slightly lower binding of tau to microtubules was observed [$\sim 75\%$; (17)]. This may be due to the fact that photobleaching requires harsher conditions than photoactivation that results in significant protein denaturation and functional impairment. In agreement, generally higher diffusion constants were observed in the FRAP study compared with our photoactivation experiment (3 versus $0.8 \mu\text{m}^2/\text{second}$ for full-length tau). Experiments, in which the mobility of GFP variants has been determined in the nucleus,

did not reveal clear differences between the different experimental approaches. Here, diffusion coefficients of 20–87 $\mu\text{m}^2/\text{second}$ have been reported for FRAP experiments, whereas 19–41 $\mu\text{m}^2/\text{second}$ have been found in a photoactivation approach (26,38,39). Thus, although FRAP and photoactivation experiments appear to give comparable diffusion coefficients for freely diffusing molecules, photoactivation may be preferable for the analysis of intracellular interactions due to the possibility to use milder conditions as lower energy is required for photoactivation compared with photobleaching.

We did not find evidence for active transport/reaction in our cell model. In some studies, it has been shown that tau is a component of slow axonal transport *in situ* and velocities between 0.2 and 3 mm per day have been reported (29–32). It is possible that slow axonal transport is evident only in longer axons or in other systems as the presence and extent of slow axonal transport of microtubule proteins appear to greatly vary with the cell types analyzed (40).

The fact that microtubules mediate the rapid distribution of tau in neurites, as documented by our data, is one facet of neuronal tau dynamics, the other one, how fresh tau molecules are supplied to the axon has recently been addressed by Konzack et al. (17). They reported a cotransport of tau with microtubule fragments that was directed from the cell body into the axon. Dynamic microtubule interaction and distal enrichment would then provide a mechanism how tau is eventually confined to and distributed in the axon in a phosphorylation-dependent manner as shown in the present work.

In this study, we have shown for the first time that tau's amino terminal projection domain mediates binding and enrichment of tau at distal neurites (Figures 5 and S2). The most characteristic feature indicating enrichment at the tip was the presence of a local minimum between enrichment and activation zone which cannot be simulated by isotropic diffusion alone and which was not present with a cytosolic control protein of similar size (3XPAGFP). The extent of distal enrichment varied between cells and was strongest in neurites with large growth cones. This suggests that a growth cone component acts as an adsorber for tau via binding to tau's amino terminal projection domain. Previously, we have shown that tau's projection domain binds to a neuronal membrane component and that this binding may be responsible for the proximodistal gradient that tau exhibits in developing axons (41,42). The binding appears to be specific because it was not observed with a cytosolic control protein and did not occur with the PHP-tau mutant, which is deficient in binding to the membrane (43). The binding either may occur to a component which is selectively enriched in the axonal tip or tau may bind in a phosphorylation-dependent manner to an uniformly distributed component as phosphorylation of tau also exhibits a graded distribution in the axon and membrane association is dependent on

tau's phosphorylation state (3). It should, however, be noted that the interaction appears to be weak and will only in combination with microtubule binding lead to a permanent enrichment at the distal neurite. Thus, it will be difficult to identify tau's interaction partner using biochemical approaches.

In vitro, several tau interaction partners have been identified some of which are components of the plasma membrane or the submembrane cortex [for review, see Brandt and Leschik (44)]. These include phosphatidylinositol (45), arachidonic acid (46) and the plasma-membrane-associated protein spectrin (47). It remains to be shown whether any of these tau interactors is involved in the transient trapping of tau at the distal neurite and whether the interaction occurs through tau's amino terminal projection domain.

Why should tau, a potent inducer of microtubule assembly, be localized to the growth cone? It is known that dynamic microtubules are present in the growth cone and that microtubules may have a decisive role in growth cone orientation. In cultured neurons, tau exhibits a proximo-distal phosphorylation gradient (41) which results in a gradient of axonal tau binding with tau being most concentrated at the transition from the axonal shaft to the growth cone (42). Because it has been shown that tau stabilizes microtubules by preserving their dynamicity (48) and increases microtubule rigidity (49), it would be perfectly positioned to contribute to the generation of a rigid but still dynamic microtubule array at the proximal growth cone important for growth cone steering. A function of tau in the growth cone is also supported by the finding that a local knockout of tau decreases lamellipodial size in the growth cone (50).

Treatment with taxol resulted in a detachment of tau from microtubules which decreased the fraction of microtubule-associated tau by almost 20%. It appears surprising that a microtubule-stabilizing agent that is frequently used in cell-free assays to determine association constants of microtubule-binding proteins reduces tau binding in cells. However, our results are in agreement with a previous study where it has been reported that treatment of cells with taxol induces detachment of tau from microtubules within minutes (35). It is known that taxol induces structural changes in the microtubule lattice (51,52). The data suggest that taxol-induced changes in microtubule structure affect binding of MAPs which should be considered when using taxol in binding assays. However, the effect of taxol to detach tau from cellular microtubules provides a tool to increase the amount of unbound tau to follow the motion and behavior of free tau as has been done in our study.

Disease-relevant conditions such as experimentally induced hyperphosphorylation or treatment with A β reduce microtubule binding and abolish distal enrichment, whereas taxol increases the effective diffusion coefficient

and permits distal enrichment (Figure 6). This indicates that microtubule interaction and distal enrichment are structurally and functionally independent which correlates with our previous observation that tau's membrane association and activity on microtubule assembly are distinct and are differentially affected by phosphorylation (43). Such a mechanism may have several consequences which are relevant for tau's distribution and its role during AD. First, differential regulation of tau's microtubule interaction and distal binding by site-specific phosphorylation provides a mechanism to generate gradients of differentially phosphorylated tau isoforms in the axon that have been reported previously (3,41). Second, phosphorylation or structural changes similar to disease-like modified PHP-tau or tau in OA-treated cells directly lead to a redistribution of tau from the axon to the somatodendritic compartment by detaching tau from microtubules and abolishing distal binding. Thus, microtubule-modulating agents that increase tau's interaction with microtubules and reduce its diffusivity may be active in suppressing neurodegenerative changes.

Materials and Methods

Materials and antibodies

Chemicals were purchased from Sigma (Deisenhofen). Cell culture media and supplements were obtained from Sigma and Invitrogen (Gaithersburg), culture flasks, plates and dishes from Nunc (Roskilde), unless stated otherwise. The following antibodies were used. Tau-5 (mouse; PharMingen), anti-GFP (rabbit; Molecular Probes Inc.), anti-tubulin (DM1A), anti-acetylated tubulin (6-11B-1). As secondary antibodies, Cy3-coupled donkey anti-mouse and donkey anti-rabbit (Dianova) and peroxidase-conjugated anti-mouse and anti-rabbit antibodies (Jackson ImmunoResearch Laboratories) were used.

Construction of expression vectors and transfections

Eukaryotic expression plasmids for fetal (352 amino acids) human tau with N-terminally fused PAGFP were constructed in pRc/CMV-based expression vectors (Invitrogen) containing a CMV promoter and ampicillin and neomycin resistance genes. PAGFP sequence was constructed from enhanced green fluorescent protein (eGFP) sequence by changing the codons L64F, T65S, V163A, T203H by site-directed mutagenesis with primers as described by (18) and cloned in pRC/CMV-FLAG-wt tau (53) to produce pCMV-PAGFP-wt tau. To construct pPAGFP-PHP tau and pPAGFP-Δtau, the respective FLAG-tau containing vectors (53) and a vector with a truncated tau sequence (pRC/CMV-FLAG-tauN223) were sequentially cut with *SacI* and *NdeI* to remove the initial segment and used as vectors for the PAGFP-tau fragment which was cut with the same enzymes. PHP tau was constructed by changing the codons for S198, S199, S202, T231, S235, S396, S404, S409, S413, and S422 to glutamate as described earlier (54) as we showed previously that tau constructs in which serine/threonine residues (which are phosphorylated to a high extent in AD tau) were substituted with glutamate to create a pseudohyperphosphorylation mimic key structural and functional aspects of hyperphosphorylated tau protein (3,43,54). To construct a 3xPAGFP control, PAGFP sequence was excised from pCMV-PAGFP-wt tau and cloned into pEGFP-C1 vector using *BglIII* and *NheI* to obtain pPAGFPx1-C1. A second *BglIII* site was added by PCR. The amplified fragment was cut with *BglIII* and inserted in pCMV-PAGFP-wt tau at *BglIII* and *BamHI* compatible sites yielding pPAGFPx2. pPAGFPx2 was digested with *BglIII* treated with CIP and used for new insertion of a amplified PAGFP fragment cut with *BglIII* to yield pPAGFPx3. Sequences that were introduced by PCR were verified by DNA sequencing.

Transfections of PC12 cells were performed with Lipofectamin 2000 (Invitrogen) essentially as described previously (53). For generation of stable lines, individual clones were selected in the presence of 500 μg/mL Geneticin, then picked and propagated in serum-DMEM supplemented with 250 μg/mL Geneticin on collagen-coated culture dishes as described previously (2). For each construct, several independent clonal lines were selected that expressed comparable levels of the protein. Transfections of primary cultures were performed 8 days after plating with Lipofectamine 2000 essentially as described previously (55) except that MEM alone was used as transfection medium.

Cell culture

PC12 cells were cultured in serum-DMEM as described previously (53). For stable lines, 250 μg/mL Geneticin were included in the medium. Undifferentiated cells were plated on 35-mm polylysine- and collagen-coated glass-bottom culture dishes (MatTek Corporation) at 1×10^3 cells/cm² and cultured in DMEM with 1% (v/v) serum. Cells were flattened by addition of 100 ng/mL 7S mouse NGF (Alomone Labs) for 1–2 days. For neuronal differentiation, NGF treatment was extended to 4–6 days and the medium was changed every 2–3 days. Before imaging, the medium was exchanged against the same medium containing DMEM without Phenol red. Primary cortical cultures were prepared from cerebral cortices of mouse embryos (day 15–17 of gestation) and cultured as described by Leschik et al. (34). The cultures were obtained by breeding C57BL/6 NCrL (Charles River Laboratories, Inc.) and C57BL/6 Jico (Harlan Winkelmann GmbH) mice. Cells were plated at 4×10^4 cells/cm² on polylysine- and laminin-coated 35-mm glass-bottom culture dishes. Colchicine treatment was performed for 30 min at 0.1 μM, taxol (Paclitaxel) was present for 1 h at 1 μM, and okadaic acid for 30 min at 10 nM. For treatment with Aβ, Aβ(1–42) (Bachem) was preaggregated at 37°C for 3 days at a concentration of 400 μM and added at a final concentration of 1 μM for 15 min to the cultures as previously described (34). Treatment with iodoacetic acid was for 30 min at 0.5 mM.

Immunocytochemistry

To reveal association of tau with microtubules, a combined Nonidet P-40 detergent extraction–fixation procedure as described previously (56) was used. To analyze distribution of endogenous tau and transfected constructs in fixed cells, cells were treated with 4% (w/v) formaldehyde in PBS as described previously (53). Staining was performed essentially as described earlier (56) in PBS containing 1% (w/v) bovine serum albumin using the respective antibodies.

Photoactivation and live imaging

Imaging was performed on a Nikon laser scanning microscope (Nikon Eclipse TE2000-U inverted), equipped with a C1 confocal laser scanning unit, argon (Ar; 488 nm), Helium/Neon (He/Ne; 543 nm) and blue diode (405 nm) lasers and EZ-C1 software. Cells were visualized using the 488 nm argon laser line and 510–540 nm band-pass emission filter. Microscope objectives used were an oil-immersion Nikon Plan Fluor 60× (NA: 1.4) UV-corrected (VC) objective. The microscope was enclosed in an incubation chamber maintained at 37°C and 5% CO₂ (Solent Scientific Limited). For automated image acquisition a macro was programmed in visual basic in the EZ-C1 software. Images were collected at 256 × 256 pixels. The following steps were performed in a photoactivation experiment. A cell was selected in the field of view and a 'preactivation image' at 488 nm excitation saved. The scan window was reduced to an 'activation spot' with a 5-μm diameter (corresponding to 130 pixels) and photoactivation was performed with the 405 nm blue diode with two scans at a pixel dwell time of 4.08 microseconds (corresponding to a total activation time in the spot of 1.1 milliseconds). The scan window was increased to the initial size and the first scan was performed after 1 second with the 488 nm laser at lowest practical laser intensity (neutral density filter of 8). Subsequent frames were obtained at a frequency of 1 frame/second and 50 or 112 frames were collected per experiment. For some experiments, the frequency of image acquisition was reduced to 1

frame/5 seconds or to 1 frame/min. It was verified by software tools that no pixels in the initial frames were saturated and movies including the preactivation image were created in 12-bit format.

Image analysis

For image analysis, a program in MATLAB was developed. The program processed the movies in the following way. The contour of the cell was recognized and the individual images were processed by Gaussian 2D-filtering (two pixels width). An offset correction was performed by subtracting the first frame ('preactivation' image) from all subsequent frames. The whole cell or part of the cell (i.e. a single neurite) was selected as 'region of interest' (ROI) by a mask technique. The ROI was kept at the same position for all frames. A 'center of intensity' (CI) was calculated analogous to computing a center of gravity and a 'momentum of intensity tensor' (TI) was calculated analogous to the momentum of inertia. TI was transformed to CI-coordinates by using the theorem of Steiner. Calculating the eigenvectors of TI yielded the main axes system (TIS). TIS was calculated for the first post-activation frame only and was used unaltered for all following frames. The major axis of TIS exhibits the lowest (quadratic) intensity spread in the direction perpendicular to it. Therefore, this axis was used as a projection axis and a coordinate x was defined along it. The valid x -range, that is, inside the ROI, was divided into 100 channels and the mean intensity per pixel was computed for each stripe perpendicular to x and corresponding to a channel. In this way, the linear distribution $I(x)$ was calculated for every frame. For an elongated neurites, for example, $I(x)$ represents the intensity density (per pixel) projected to the neurite's axis. The data were plotted as a color-coded filled contour plot of the 2D intensity function $I(x, t)$, where t is the time in seconds. The color scale ranges from red (highest intensity) to violet (zero). This plot provides a visual representation of the dissipation and movement of the photoactivated molecules from the activated segment. Intensities were normalized for the total photoactivated population that was detected in the ROI of the first frame after dark frame correction. To quantitate the intensity decay in the activated segment, the region of activation $x_A \pm w$ was selected in the first frame post-activation and the intensity in this region was averaged using $I(x)$ for each frame. To compare the dissipation of different constructs and at different conditions, I_{10}/I_{tot} from the fluorescence intensity averaged over w at 10 second post-activation (I_{10}) in the activated segment and the fluorescence signal from the total photoactivated population (I_{tot}) was operationally defined. This value reflects the immobile fraction of the activated population in the activated segment after 10 seconds.

Modelling and simulation

To determine the behavior of the constructs, a diffusion model solving Fick's second diffusion equation was developed and used to fit the data from the photoactivation experiments. A neurite was considered to be a tube with one closed end. With the method of 'images', the analytical solution for the normalized intensity in the activation region $x_A \pm w$ can be given as:

$$I(t) = \frac{e^{-\lambda \cdot t}}{\sqrt{2\pi\sigma}} \left(1 + e^{-\frac{4(x_A - x_T)^2}{2\sigma^2}} - e^{-\frac{4(x_A - x_B)^2}{2\sigma^2}} \right) + o \quad (1)$$

and

$$\sigma = \sqrt{2Dt + \sigma_0^2} \quad (2)$$

[with t = time (seconds), x_A = position of activation, x_T = position of tip, x_B = position of cell body, σ_0 = width of $I(x, t = 0)$, o = offset parameter, D = diffusion coefficient]. Photobleaching was set as $\lambda = 0.001/\text{second}$ as determined from control experiments. Starting values σ_0 and o were calculated from the intensity distribution $I(x)$ of the first frame according to:

$$I(x) = \frac{1}{\sqrt{2\pi\sigma_0}} e^{-\frac{(x-x_A)^2}{2\sigma_0^2}} + o. \quad (3)$$

The resulting parameters were used for simulations of $I(x, t)$ (see e.g. Figure 2B, bottom). In these simulations, also defined background noise was introduced to facilitate comparison with experiment.

Other methods

Immunoblot analysis and quantification of the blots was performed as described previously (34). Data were expressed as means \pm S.E. Statistical analysis among experimental groups was performed using paired Student's t test (Origin 7.0) or one-way ANOVA followed by *post hoc* Bonferroni test. p values are *, $p < 0.05$; **, $p < 0.01$; ***, $p < 0.001$.

Acknowledgments

We thank Dr Robert Stad, Dr Marteen Balzar and Kees van der Oord (all from Nikon, Amsterdam) for their kind help in the setting of the microscope system. We also thank Lidia Bakota for helpful suggestions on the manuscript. This work was supported by the Ministry for Science and Culture of Lower Saxony and a fellowship of the graduate college 612 of the Deutsche Forschungsgemeinschaft (CW).

Supporting Information

Additional Supporting Information may be found in the online version of this article:

Contour and color coded plots of 2D intensity functions from five representative cells per condition in which the indicated constructs have been activated in the middle of the process. Position of activation (arrow) and tip of process (arrowhead) is indicated. The field of view is $100 \times 100 \mu\text{m}$ with 256×256 pixel resolution. The projection coordinate is given in pixel.

Figure S1: PC12 cells stably expressing PAGFP-wt tau.

Figure S2: PC12 cells stably expressing PAGFP-tau Δ .

Figure S3: PC12 cells stably expressing 3XPAGFP.

Figure S4: PC12 cells stably expressing PAGFP-wt tau treated with taxol.

Figure S5: PC12 cells stably expressing PAGFP-tau Δ treated with OA.

Figure S6: PC12 cells stably expressing PAGFP-tau Δ treated with preaggregated A β .

Please note: Wiley-Blackwell are not responsible for the content or functionality of any supporting materials supplied by the authors. Any queries (other than missing material) should be directed to the corresponding author for the article.

References

- Shahani N, Brandt R. Functions and malfunctions of the tau proteins. *Cell Mol Life Sci* 2002;59:1668–1680.
- Brandt R, Leger J, Lee G. Interaction of tau with the neural plasma membrane mediated by tau's amino-terminal projection domain. *J Cell Biol* 1995;131:1327–1340.
- Maas T, Eidenmuller J, Brandt R. Interaction of tau with the neural membrane cortex is regulated by phosphorylation at sites that are modified in paired helical filaments. *J Biol Chem* 2000;275:15733–15740.
- Goedert M, Spillantini MG. A century of Alzheimer's disease. *Science* 2006;314:777–781.

5. Ballatore C, Lee V, Trojanowski J. Tau-mediated neurodegeneration in Alzheimer's disease and related disorders. *Nat Rev Neurosci* 2007;8:663–672.
6. Stokin GB, Lillo C, Falzone TL, Brusch RG, Rockenstein E, Mount SL, Raman R, Davies P, Masliah E, Williams DS, Goldstein LS. Axonopathy and transport deficits early in the pathogenesis of Alzheimer's disease. *Science* 2005;307:1282–1288.
7. Baas PW, Vidya Nadar C, Myers KA. Axonal transport of microtubules: the long and short of it. *Traffic* 2006;7:490–498.
8. Kanai Y, Hirokawa N. Sorting mechanisms of tau and MAP2 in neurons: suppressed axonal transit of MAP2 and locally regulated microtubule binding. *Neuron* 1995;14:421–432.
9. Hirokawa N, Funakoshi T, Sato-Harada R, Kanai Y. Selective stabilization of tau in axons and microtubule-associated protein 2C in cell bodies and dendrites contributes to polarized localization of cytoskeletal proteins in mature neurons. *J Cell Biol* 1996;132:667–679.
10. Litman P, Barg J, Rindzoonki L, Ginzburg I. Subcellular localization of tau mRNA in differentiating neuronal cell culture: implications for neuronal polarity. *Neuron* 1993;10:627–638.
11. Stamer K, Vogel R, Thies E, Mandelkow E, Mandelkow EM. Tau blocks traffic of organelles, neurofilaments, and APP vesicles in neurons and enhances oxidative stress. *J Cell Biol* 2002;156:1051–1063.
12. Dixit R, Ross JL, Goldman YE, Holzbaur EL. Differential regulation of dynein and kinesin motor proteins by tau. *Science* 2008;319:1086–1089.
13. Cuchillo-Ibanez I, Seereeram A, Byers HL, Leung KY, Ward MA, Anderton BH, Hanger DP. Phosphorylation of tau regulates its axonal transport by controlling its binding to kinesin. *FASEB J* 2008;22:3186–3195.
14. Falzone TL, Stokin GB, Lillo C, Rodrigues EM, Westerman EL, Williams DS, Goldstein LS. Axonal stress kinase activation and tau misbehavior induced by kinesin-1 transport defects. *J Neurosci* 2009;29:5758–5767.
15. Waters JC. Live-cell fluorescence imaging. *Methods Cell Biol* 2007;81:115–140.
16. Weissmann C, Brandt R. Mechanisms of neurodegenerative diseases: insights from live cell imaging. *J Neurosci Res* 2008;86:504–511.
17. Konzack S, Thies E, Marx A, Mandelkow EM, Mandelkow E. Swimming against the tide: Mobility of the microtubule-associated protein tau in neurons. *J Neurosci* 2007;27:9916–9927.
18. Patterson G, Lippincott-Schwartz J. A photoactivatable GFP for selective photolabeling of proteins and cells. *Science* 2002;297:1873–1877.
19. Ferenz NP, Wadsworth P. Prophase microtubule arrays undergo flux-like behavior in mammalian cells. *Mol Biol Cell* 2007;18:3993–4002.
20. Shahani N, Subramaniam S, Wolf T, Tackenberg C, Brandt R. Tau aggregation and progressive neuronal degeneration in the absence of changes in spine density and morphology after targeted expression of Alzheimer's disease-relevant tau constructs in organotypic hippocampal slices. *J Neurosci* 2006;26:6103–6114.
21. Porzig R, Singer D, Hoffmann R. Epitope mapping of mAbs AT8 and Tau5 directed against hyperphosphorylated regions of the human tau protein. *Biochem Biophys Res Commun* 2007;358:644–649.
22. Ferreira A, Busciglio J, Caceres A. Microtubule formation and neurite growth in cerebellar macroneurons which develop in vitro: evidence for the involvement of the microtubule-associated proteins, MAP-1a, HMW-MAP2 and Tau. *Brain Res Dev Brain Res* 1989;49:215–228.
23. Crank J. *The Mathematics of Diffusion*. Oxford: Oxford University Press; 2004.
24. Swaminathan R, Hoang CP, Verkman AS. Photobleaching recovery and anisotropy decay of green fluorescent protein GFP-S65T in solution and cells: cytoplasmic viscosity probed by green fluorescent protein translational and rotational diffusion. *Biophys J* 1997;72:1900–1907.
25. Sprague BL, Pego RL, Stavreva DA, McNally JG. Analysis of binding reactions by fluorescence recovery after photobleaching. *Biophys J* 2004;86:3473–3495.
26. Dross N, Spriet C, Zwerger M, Müller G, Waldeck W, Langowski J. Mapping eGFP oligomer mobility in living cell nuclei. *PLoS ONE* 2009;4:e5041.
27. Vallee R, Bloom G. Mechanisms of fast and slow axonal transport. *Annu Rev Neurosci* 1991;14:59–92.
28. Sabri M, Ochs S. Inhibition of glyceraldehyde-3-phosphate dehydrogenase in mammalian nerve by iodoacetic acid. *J Neurochem* 1971;18:1509–1514.
29. Mercken M, Fischer I, Kosik K, Nixon R. Three distinct axonal transport rates for tau, tubulin, and other microtubule-associated proteins: evidence for dynamic interactions of tau with microtubules in vivo. *J Neurosci* 1995;15:8259–8267.
30. Tashiro T, Sun X, Tsuda M, Komiya Y. Differential axonal transport of soluble and insoluble tau in the rat sciatic nerve. *J Neurochem* 1996;156:1566–1574.
31. Utton MA, Connell J, Asuni AA, van Slegtenhorst M, Hutton M, de Silva R, Lees AJ, Miller CC, Anderton BH. The slow axonal transport of the microtubule-associated protein tau and the transport rates of different isoforms and mutants in cultured neurons. *J Neurosci* 2002;22:6394–6400.
32. Zhang B, Higuchi M, Yoshiyama Y, Ishihara T, Forman MS, Martinez D, Joyce S, Trojanowski JQ, Lee VM. Retarded axonal transport of R406W mutant tau in transgenic mice with a neurodegenerative tauopathy. *J Neurosci* 2004;24:4657–4667.
33. Utton M, Noble W, Hill J, Anderton B, Hanger D. Molecular motors implicated in the axonal transport of tau and alpha-synuclein. *J Cell Sci* 2005;118:4645–4654.
34. Leschik J, Welzel A, Weissmann C, Eckert A, Brandt R. Inverse and distinct modulation of tau-dependent neurodegeneration by presenilin 1 and amyloid-beta in cultured cortical neurons: evidence that tau phosphorylation is the limiting factor in amyloid-beta-induced cell death. *J Neurochem* 2007;101:1303–1315.
35. Samsonov A, Yu J, Rasenick M, Popov S. Tau interaction with microtubules in vivo. *J Cell Sci* 2004;117:6129–6141.
36. Gamblin TC, Chen F, Zambrano A, Abraha A, Lagalwar S, Guillozet AL, Lu M, Fu Y, Garcia-Sierra F, LaPointe N, Miller R, Berry RW, Binder LI, Cryns VL. Caspase cleavage of tau: linking amyloid and neurofibrillary tangles in Alzheimer's disease. *Proc Natl Acad Sci U S A* 2003;100:10032–10037.
37. Esmaeli-Azad B, McCarty JH, Feinstein SC. Sense and antisense transfection analysis of tau function: tau influences net microtubule assembly, neurite outgrowth and neuritic stability. *J Cell Sci* 1994;107:869–879.
38. Beaudouin J, Mora-Bermudez F, Klee T, Daigle N, Ellenberg J. Dissecting the contribution of diffusion and interactions to the mobility of nuclear proteins. *Biophys J* 2006;90:1878–1894.
39. Mazza D, Braekmans K, Cella F, Testa I, Vercauteren D, Demeester J, De Smedt SS, Diaspro A. A new FRAP/FRAPa method for three-dimensional diffusion measurements based on multiphoton excitation microscopy. *Biophys J* 2008;95:3457–3469.
40. Okabe S, Hirokawa N. Differential behavior of photoactivated microtubules in growing axons of mouse and frog neurons. *J Cell Biol* 1992;117:105–120.
41. Mandell J, Banker G. A spatial gradient of tau protein phosphorylation in nascent axons. *J Neurosci* 1996;16:5727–5740.
42. Kempf M, Clement A, Faissner A, Lee G, Brandt R. Tau binds to the distal axon early in development of polarity in a microtubule- and microfilament-dependent manner. *J Neurosci* 1996;16:5583–5592.
43. Eidenmuller J, Fath T, Maas T, Pool M, Sontag E, Brandt R. Phosphorylation-mimicking glutamate clusters in the proline-rich region are sufficient to simulate the functional deficiencies of hyperphosphorylated tau protein. *Biochem J* 2001;357:759–767.
44. Brandt R, Leschik J. Functional interactions of tau and their relevance for Alzheimer's disease. *Curr Alzheimer Res* 2004;1:255–269.
45. Surridge CD, Burns RG. The difference in the binding of phosphatidylinositol distinguishes MAP2 from MAP2C and tau. *Biochemistry* 1994;33:8051–8057.
46. Wilson DM, Binder LI. Free fatty acids stimulate the polymerization of tau and amyloid beta peptides. In vitro evidence for a common effector of pathogenesis in Alzheimer's disease. *Am J Pathol* 1997;150:2181–2195.

47. Carlier MF, Simon C, Cassoly R, Pradel LA. Interaction between microtubule-associated protein tau and spectrin. *Biochimie* 1984;66:305–311.
48. Kaech S, Ludin B, Matus A. Cytoskeletal plasticity in cells expressing neuronal microtubule-associated proteins. *Neuron* 1996;17:1189–1199.
49. Felgner H, Frank R, Biernat J, Mandelkow EM, Mandelkow E, Ludin B, Matus A, Schliwa M. Domains of neuronal microtubule-associated proteins and flexural rigidity of microtubules. *J Cell Biol* 1997;138:1067–1075.
50. Liu CW, Lee G, Jay DG. Tau is required for neurite outgrowth and growth cone motility of chick sensory neurons. *Cell Motil Cytoskeleton* 1999;43:232–242.
51. Xiao H, Verdier-Pinard P, Fernandez-Fuentes N, Burd B, Angeletti R, Fiser A, Horwitz SB, Orr GA. Insights into the mechanism of microtubule stabilization by taxol. *Proc Natl Acad Sci U S A* 2006;103:10166–10173.
52. Nogales E, Wolf SG, Khan IA, Luduena RF, Downing KH. Structure of tubulin at 6.5 Å and location of the taxol-binding site. *Nature* 1995;375:424–427.
53. Fath T, Eidenmuller J, Brandt R. Tau-mediated cytotoxicity in a pseudohyperphosphorylation model of Alzheimer's disease. *J Neurosci* 2002;22:9733–9741.
54. Eidenmuller J, Fath T, Hellwig A, Reed J, Sontag E, Brandt R. Structural and functional implications of tau hyperphosphorylation: information from phosphorylation-mimicking mutated tau proteins. *Biochemistry* 2000;39:13166–13175.
55. Wiegert JS, Bengtson CP, Bading H. Diffusion and not active transport underlies and limits ERK1/2 synapse-to-nucleus signaling in hippocampal neurons. *J Biol Chem* 2007;282:29621–29633.
56. Lee G, Rook SL. Expression of tau protein in non-neuronal cells: microtubule binding and stabilization. *J Cell Sci* 1992;102:227–237.